Journal of
Applied Crystallography

ISSN 0021-8898

Received 16 August 2006
Accepted 27 February 2007

Biological small-angle X-ray scattering facility at the Stanford Synchrotron Radiation Laboratory

Igor L. Smolsky,[a] Ping Liu,[a] Marc Niebuhr,[a] Kazuki Ito,[a,b] Thomas M. Weiss[a] and Hiro Tsuruta[a]*

[a]Stanford Synchrotron Radiation Laboratory, Stanford Linear Accelerator Center, Stanford University, Menlo Park, California, USA, and [b]The Institute of Physical and Chemical Research (RIKEN), Harima Institute SPring-8 Center, Structural Materials Science Laboratory, 1-1-1 Kouto, Sayo-cho, Sayo-gun, Hyogo, Japan. Correspondence e-mail: tsuruta@slac.stanford.edu

Beamline 4-2 at the Stanford Synchrotron Radiation Laboratory is a small-angle X-ray scattering/diffraction facility dedicated to structural studies on mostly noncrystalline biological systems. The instrument consists of a pinhole camera, which covers the magnitude of the scattering vector Q in the range 0.004–1.3 Å^{-1} [$Q = (4\pi/\lambda)\sin\theta$, where θ and λ are one half of the scattering angle and the X-ray wavelength, respectively], and a Bonse–Hart geometry ultra-small-angle X-ray scattering setup for the Q range an order of magnitude smaller. The pinhole camera allows quick automated distance and detector selection among any combination of five distances and three position-sensitive detectors. The double-crystal monochromator can have either Si 111 crystals or a pair of synthetic multilayer diffractive elements for higher flux applications. We have adopted a suite of software originally developed for macromolecular crystallography for integrated beamline control as well as static and slow time-resolved small-angle scattering data collection. This article outlines recent technological developments and specialized instrumentation for conducting noncrystalline scattering experiments in structural biology at improved time and spatial resolutions.

© 2007 International Union of Crystallography
Printed in Singapore – all rights reserved

1. Introduction

The majority of small-angle X-ray scattering (SAXS) experiments deal with noncrystalline or partially oriented particles of colloidal characteristic lengths. The scattering signal from one particle is incoherent with respect to that from another so that the signal level is usually very weak. Scattering profiles from these systems usually lack dominant features such as diffraction spots from crystals. In the case of solution X-ray scattering, the source of scattering is a small difference in electron density, commonly called 'contrast', between solute and solvent. The majority of biological substances consist of low atomic number elements, and require water to maintain their biological functions, resulting in low contrast. The development of specialized instrumentation is required to accurately extract a very weak signal above the water scattering and instrument background. A number of excellent reviews have appeared (*e.g.* Koch *et al.*, 2003) outlining this class of experiment and applications in structural biology.

Beamline 4-2 (BL4-2) at the Stanford Synchrotron Radiation Laboratory (SSRL) was built in the early 1980s originally as a multipurpose X-ray station on the central fan of the radiation from an electromagnet wiggler on the Stanford Positron Electron Accelerating Ring (SPEAR). Late in the 1980s a compact small-angle scattering instrument was set up on BL4-2 for a number of noncrystalline diffraction studies (Wakatsuki *et al.*, 1992). Another generation of small-angle scattering instrument, featuring a sectioned large diameter vacuum flight path and gas chamber detectors, was built and permanently installed on BL4-2 shortly after the low-emittance storage ring upgrade (SPEAR2) early in the 1990s to meet unique technological challenges and increasing user demand in biological small-angle scattering studies. We recently built the third-generation instrument, optimized for structural biology studies, to take full advantage of the lower emittance beam provided by the third-generation storage ring SPEAR3 and successfully commissioned it in 2005. Here we report the characteristics and capabilities of the new instrument on BL4-2.

2. Optics

2.1. Wiggler source

The original eight-pole electromagnet wiggler was replaced by the 2.0 T 20-pole permanent magnet wiggler, first operated in 2004. The 0.5 mrad central fan of the wiggler radiation is used for most experiments on BL4-2. The wiggler field is currently limited to 0.66 T primarily because the existing optic components, which were built before the SPEAR2 upgrade, can not take the high thermal load that would be imposed by the full field wiggler operation. The full field operation will commence as soon as we complete the optics upgrade project in late 2007.

2.2. Focusing mirror

Beam focusing is achieved by a bent cylinder mirror made of single-crystal silicon. The mirror, coated with Pt, sets the energy cut-off approximately at 11.5 keV. It is located at 13.5 m from the source point, providing an approximately 1:1 image of the wiggler source

near the detector position. During the SPEAR3 upgrade, a water-cooled metal block was added to the mirror bender to help dissipate additional heat load to improve the thermal stability of the mirror, which previously had no active cooling. The mirror temperature remains at 315 ± 1 K regardless of the ring current. The top-up-mode storage ring operation (100–85 mA) also contributes positively to the nearly constant thermal load on the mirror, which is exposed to the wiggler radiation at all times except during the top-up, which typically lasts only 1–2 min.

2.3. Monochromator

BL4-2 is equipped with the Howard–Brown design double-crystal monochromator, which is common among tunable hard X-ray experimental stations built before the SPEAR2 upgrade at SSRL. The monochromator employs a pair of asymmetrically cut Si 111 crystals, and provides a typical energy band pass $\Delta E/E \simeq 5 \times 10^{-4}$, suitable for absorption spectroscopy and anomalous scattering studies. An optional pair of synthetic multilayer diffractive elements, on the other hand, gives ~2% full width at half maximum (FWHM) band pass, providing 20–30 times higher flux level without noticeable broadening of the sharpest fiber diffraction peaks (Tsuruta, Brennan *et al.*, 1998). The pair of multilayer diffractive elements, each composed of 150 layer pairs of W/B_4C deposited on a silicon crystal substrate, replace the Si 111 crystals on regular basis in fast time-resolved studies on the millisecond timescale. A water-cooled metal block is attached to either of the upstream monochromator elements for thermal management. The characteristics of the multilayer beam have been fully described elsewhere (Tsuruta, Brennan *et al.*, 1998).

2.4. Overall beam characteristics

The SPEAR3 upgrade improved the electron beam emittance from 160 to 18 nm rad. The new wiggler now provides a beam intensity profile narrower than in the past by a factor of 4–5. The usable beam flux is higher by a factor of 2–3 due to the much smaller primary beam size, even with the lower wiggler field. We routinely obtain an FWHM beam size of 0.2 mm vertical and 1.0 mm horizontal at the focal plane near the detector position with the 0.5 mrad horizontal mirror acceptance, and record beam flux of approximately 10^{11} photons s^{-1} at 9 keV with Si crystals and 3×10^{12} photons s^{-1} with the multilayers. These values are expected to increase by at least an order of magnitude with the full field wiggler operation and SPEAR3 500 mA operation in 2007. Our beam imager, composed of a scintillator screen, prism, microscope objective lens and sensitive charge-coupled-device (CCD) video camera, provides a quick and convenient means of evaluating beam focus quality. The automated real-time digitization and evaluation of the beam profile in FWHM, including Gaussian fit, has been implemented *via* the use of a frame grabber plug-in within *ImageJ* (National Institutes of Health, 2004).

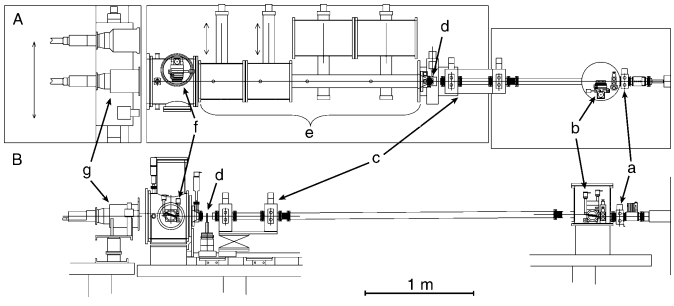

Figure 1
The third-generation instrument on SSRL BL4-2. A: a top view of the instrument in transition from 2.5 to 1.5 m distance (a: defining slit; b: USAXS collimator crystal; c: guard slit assemblies; d: sample stage; e: adjustable beam flight path; f: USAXS analyzer crystal; g: detector stage). B: a side view of the instrument in the 0.5 m configuration with the USAXS setup in place. The motorized vertical translation deploys the USAXS crystals, which are otherwise moved out of the beam for the pinhole camera. The experimental tables are translated vertically to compensate for the different beam height downstream of each crystal.

3. Instrument capabilities

3.1. New flight path with automated distance change

The choice of suitable angular range depends on the characteristic lengths of the system to be studied and the type of structural information desired. More than a single sample-to-detector distance is often required for a set of experiments. One of the technical goals of building the new instrument was to provide rapid and effortless distance change. This capability has become increasingly important in recent years to achieve improved efficiency in data collection, as a shorter beam-time slot is given to each user group in order to accommodate the ever-growing user population in structural biology. Renewed interests in working at higher scattering angles among the solution scattering community call for the use of a distance much shorter than had been typically used (Petoukhov *et al.*, 2002; Fischetti *et al.*, 2003; Hirai *et al.*, 2002; Zuo *et al.*, 2006). The advanced detector technologies and stable high-flux beams available at many synchrotron facilities are indeed making high-angle studies around the magnitude of the scattering vector $Q = 1$ Å^{-1} or higher a routine practice [$Q = (4\pi/\lambda)\sin\theta$, where θ and λ are one half of the scattering angle and the X-ray wavelength, respectively]. There are a few different approaches to make available multiple Q ranges within a short beam-time slot. A special upstream pipe with a window for a second detector has been developed to cover higher angles simultaneously with low scattering angles (Rapp *et al.*, 1995). Our second-generation instrument was equipped with a similar upstream pipe, which unfortunately did not meet the increasing demands for covering larger azimuthal scattering angles in biology. The distance change in small-angle scattering experiments is achieved in most cases by relocating either the sample stage or the detector along the beam axis. In either case, any new air gap must be evacuated to become a part of the beam flight path. We opted for relocating the sample stage in favor of keeping the same beam focus position, since that eliminates additional effort for focus adjustment, beam-stop alignment and the need for detector containment inside the vacuum path (Boesecke & Diat, 1997). This approach is more suitable for our routine operation, which involves three different types of detectors to meet specific experimental requirements, and also better protects our detectors, which are costly to replace.

The new instrument incorporates an evacuated flight path, made up of five sections, slit assemblies, a sample stage, detectors and a beam stop (Fig. 1). All but the most downstream section are mounted on horizontal motorized slides for rapid distance change. The downstream section incorporates the ultra-small-angle X-ray scattering (USAXS) analyzer crystal on a vertical translation stage as well as an interchangeable beam stop with an incorporated photodiode for recording transmitted beam intensity. Each of the pipe sections has an NW320 ISO flange on both ends and an O-ring seal on one end to achieve a vacuum seal through mild compression by the most upstream vacuum flange, which is mounted on a long motorized slide together with the sample stage and slit assemblies. The pipe sections are also equipped with a spring-loaded translation mechanism in the beam direction so that they spontaneously separate

Table 1
Range of Q and corresponding Bragg spacing (D) typically covered by different instrument configurations at the photon energy of 9 keV using the MarCCD165 detector.

Actual values depend on exact experimental geometry, sample scattering cross section, beam stability and detector spatial resolution.

	Q_{min} [Å^{-1}], (D_{max} [Å])		Q_{max} [Å^{-1}], (D_{min} [Å])	
	Beam stop diameter		Detector position	
Setup	4 mm	7 mm	Centered	Off-centered
0.5 m	0.032 (195)	0.046 (135)	0.68 (9)	1.33 (5)
1 m	0.015 (420)	0.022 (290)	0.34 (18)	0.68 (9)
1.5 m	0.009 (700)	0.014 (450)	0.23 (28)	0.45 (13)
2 m	0.006 (1050)	0.009 (700)	0.17 (37)	0.34 (18)
2.5 m	0.004 (1570)	0.007 (890)	0.14 (46)	0.27 (23)
Fiber diffraction	0.025 (251)		1.43 (4)	2.60 (2.4)
USAXS	0.00063 (9980)		0.02 (314)	

from one another when the vacuum flange is moved upstream by a few centimetres after venting the vacuum. The 2.5 m distance requires all five vacuum pipe sections, while the 1.5 m distance, as illustrated in Fig. 1A, requires three of the five. Our beamline control program, described in §3.5 below, takes care of all required hardware translations, the operation of vacuum valves and pumps, and minimizes accidents by checking limit switch status and the position of each component.

The range of Q covered by the five different standard distances is tabulated in Table 1. The high-angle coverage can be extended further by the portable fiber diffraction setup with 23 cm scattering path, which can be installed immediately downstream of the USAXS collimator housing. The USAXS setup, described below, extends the resolution range towards larger characteristic lengths.

3.2. Incorporated ultra-small-angle scattering setup

Most synchrotron-based small-angle scattering instruments (*e.g.* Amenitsch *et al.*, 1995; Fischetti *et al.*, 2004; Narayanan *et al.*, 2001) employ the pinhole geometry with a position-sensitive detector. Principal motivations for this approach include (1) the use of as much available X-ray flux as possible to enhance signals from mostly weakly scattering biological samples, especially for time-resolved studies; and (2) the need to obtain two-dimensional scattering patterns. Pinhole-geometry SAXS instruments have a typical low-Q limit in the range 0.002–0.02 Å^{-1}, depending primarily on beam characteristics and sample scattering power. Scanning instruments utilize an angular analyzer instead to achieve a superior small-angle resolution, as commonly found in USAXS instruments in Bonse–Hart geometry (Diat *et al.*, 1995; Narayanan *et al.*, 2001; Ilavsky *et al.*, 2002). A USAXS instrument has recently been adopted to perform imaging studies as a function of scattering angle, potentially opening up a new field of structural studies (Levine & Long, 2004). An increasing number of biological studies involve large macromolecular assemblies whose largest dimensions approach or surpass the low-Q limits of many pinhole-geometry instruments. We have incorporated a Bonse–Hart geometry setup to complement the capabilities of our standard pinhole-geometry instrument based on our experience in building a stand-alone USAXS setup, which also functioned as a diffraction-enhanced imaging instrument using a different set of crystals. We have adopted channel-cut Si 111 crystals with four or six reflections to simplify the experimental geometry, compared to the five-bounce geometry we had previously used. The permanent integration of these crystals into our pinhole-geometry instrument improves the availability of the USAXS setup to cover much smaller scattering angles (Fig. 1). Preliminary characteristics of the incorporated USAXS setup, which is in a process of further optimization, are given in Table 1. The shortest standard distance of 0.5 m is used to keep the beam within the small active area of the avalanche photodiode detector (APD), which maintains over six orders of magnitude of excellent photon count rate linearity. The wide detector dynamic range allows the use of minimum beam attenuation to obtain the analyzer rocking curve around the primary beam for direct beam center determination, minimizing systematic errors in intensity scaling.

3.3. Sample handling devices

The instrument is designed to cover a diverse spectrum of structural biology experiments, from completely randomly oriented systems, *i.e.* solution scattering, to partially and highly oriented systems such as fibers, lipid membranes and single crystals. Each different class of specimen requires a specific sample holder, and there are additional requirements including temperature and humidity control as well as altering sample orientation during data collection. We have developed disposable polycarbonate sample cuvettes for protein solution scattering, which is the most common class of experiment at BL4-2. A pair of 10 µm thick mica windows are glued on each side of the cuvette and a 12 µl sample aliquot is injected using a microsyringe. The cuvette is then placed in a thermostated holder, which has dry nitrogen purging to prevent moisture condensation on the cell windows at temperatures below the dew point. The cuvette holder is mounted on a motorized sample stage, and allows automated data collection using up to six cuvettes in series. We have also developed three different versions of flow cells, each incorporating a quartz X-ray capillary. Two of them place the capillary completely under vacuum, minimizing the background scattering level (Dubuisson *et al.*, 1997). Any of the flow cells can be connected to a computer-controlled Hamilton ML540B liquid dispenser (Hamilton Company, Reno, NV, USA), which delivers the sample aliquot into the flow-cell capillary, and gently moves or oscillates the sample in the beam to minimize radiation damage by spreading the total radiation dosage over a larger sample volume, *i.e.*, a larger number of protein molecules. It can also be used to empty, flush or fill the capillary with buffer solution. Time-resolved studies usually require highly sophisticated sample stimulation devices specific to a particular biological system. A stopped-flow apparatus (Unisoku, Hirakata, Japan) is used for time-resolved solution scattering studies on the millisecond to minute timescale. A Huber 408 goniostat (Huber Diffraktionstechnik, Rimsting, Germany) is available for single-crystal diffraction as well as grazing-incidence scattering studies. A locking kinematic mount on the sample stage facilitates alignment upon switching to a different sample-handling device, including those supplied by external users. A magnetic sample orienter, producing 1 T in a 1 cm gap, is also available. Additional details on the sample-handling devices are provided on our web page (Stanford Synchrotron Radiation Laboratory, 2006*a*).

3.4. Detectors

Detector characteristics must match a specific set of experimental requirements. No single detector can satisfy the diverse experimental requirements in noncrystalline diffraction experiments. BL4-2 is equipped with three detector systems suitable for different classes of experiments: a position-sensitive gas detector system incorporating linear and quadrant gas proportional counters (European Molecular Biology Laboratory; Gabriel, 1977); an image-intensified CCD X-ray detector system (Hamamatsu Photonics, Hamamatsu, Japan: Amemiya *et al.*, 1995); and an optic fiber coupled CCD MarCCD165

detector (Mar USA, Evanston, IL, USA). The gas detector system provides over four orders of magnitude of dynamic range at global photon count rates up to about 100 kHz. Its superior electronic stability and extremely low noise level make it ideal for solution scattering experiments. The gas detectors, however, suffer from low detection efficiencies at higher global count rates and from the space-charge effect that limits maximum local count rates. The MarCCD165 detector complements the gas detectors in high count rate applications including membrane, fiber and single-crystal diffraction studies, many of which also require higher spatial resolution and accuracy. A series of recent hardware upgrades have made this detector highly effective for solution scattering studies in combination with its relatively large active area for azimuthal signal averaging. The image-intensified CCD system parallels the gas detectors in its sensitivity primarily due to the high gain of the Hamamatsu V7739P image intensifier. The detector system is equipped with a progressive scan interline Hamamatsu C4880-80-14A CCD camera with two registers per pixel, each for charge integration and readout. The system is capable of recording two-dimensional scattering profiles continuously at rates up to 28 Hz in the fast scan mode using the full resolution of 659 × 494 pixels. We have used up to 8 × 8 pixel binning (82 × 61 pixels) to increase the frame rate to 190 Hz in actual time-resolved protein solution scattering experiments. All these detectors, the APD detector for USAXS and the beam imager for focus optimization, are mounted on a computer-controlled horizontal translation stage for user selection.

3.5. Software developments

Developing a universal suite of data collection software for a diverse spectrum of experiments is highly challenging, yet essential for conducting experiments successfully and effectively. BL4-2 has a diverse set of hardware and software for motion control primarily due to nearly two decades of developments. Our detectors were delivered with manufacturer-provided hardware and software, requiring software and/or hardware interfaces to our motion control system. It is essential to relieve experimenters from acting as an interface to several separate programs and instead allow them to focus on data evaluation and planning for the next set of experiments. We have solved these technical challenges by adopting the distributed control system (DCS) and the accompanying graphical user interface (GUI) *Blu-ICE*, originally developed for macromolecular crystallography stations at SSRL (McPhillips *et al.*, 2002). They have also been adopted for single-crystal X-ray absorption spectroscopy (Latimer *et al.*, 2005). The DCS/*Blu-ICE* package brought a number of notable benefits including: (1) in-house origin with a large knowledge base at SSRL; (2) proven stability; (3) IP-based client/server model that allows integration of the instrument control system (ICS), which is the older beamline control program at SSRL (George, 2000); (4) remote viewing and/or control of the experiment; (5) script-based language and object-oriented architecture that facilitate customization of existing features and addition of new data collection capabilities; and (6) X-windows GUI package *Blu-ICE* that can be run on all of the common operating systems including Microsoft Windows, Linux, Unix and Macintosh OS X.

In addition to a number of highly developed features for macromolecular crystallography, we have implemented specific features for noncrystalline diffraction experiments, including: (1) automated change of sample-to-detector distance; (2) USAXS data collection with programmed filter insertion; (3) automated slit alignment; (4) automated sample alignment for the solution sample cuvette; (5) point-and-click sample alignment using a video microscope, and (6) automated data collection at up to ten sample positions. In addition, incident and transmitted beam intensities are integrated synchronously during each X-ray exposure and recorded in the header portion of the diffraction data in 16-bit TIFF as well as in an accompanying text file, along with other experimental parameters, for accurate data scaling and background subtraction. The automated distance change has been described in §3.1. The automated slit alignment procedure first opens all four slit blades in each slit, and then optimizes one blade at a time by gradually closing the blade by a predetermined step size while monitoring the transmitted beam intensity through the slit until the beam intensity drops by a predetermined value. The slit blade is opened again by a predetermined step size, and the entire step is repeated at a smaller step size for finer alignment. The automated sample alignment is achieved by maximizing the transmitted beam intensity through a small pinhole in the middle of the standard polycarbonate cuvette by scanning the sample stage in the horizontal and vertical directions. The alternative sample alignment procedure takes advantage of the video microscope specifically developed for viewing samples on axis using a penta prism and a mirror. The prism on the motorized vertical translation stage is moved into the beam axis for sample viewing. A single mouse click in the *Blu-ICE* sample viewing window aligns a desired area of the sample or one of several samples on to the crosshair which is aligned to the beam spot. Up to ten sample positions can be stored in the *Blu-ICE* sample scan tab, and a series of static measurements can be performed automatically after moving out the prism. Waiting periods can be set for time-resolved studies on slow processes.

On-site evaluation of data is indispensable for successful data collection and this should be done as soon as a set of data have been recorded. In-depth evaluation of the recorded data ensures its usefulness and guides the next set of experiments within a short beam-time slot. We have developed a data processing program which performs azimuthal averaging of two-dimensional scattering profiles into one-dimensional profiles, statistical evaluation, intensity scaling, averaging and calculating the variance of multiple data frames, background subtraction, and conversion of detector pixels to Q values. The program *MarParse* reads in a simple text file, containing data-file names and processing parameters such as averaging area and direct beam position. *MarParse* can process any 16-bit TIFF images such as those generated by the MarCCD165 and Hamamatsu CCD detectors. It evaluates data statistics upon azimuthal averaging. The program then performs pixel-by-pixel division of the averaged intensities by either incident or transmitted beam intensity integrated during each exposure. All output files are written in the ASCII format and are compatible with a number of data analysis programs. The background correction specific to the scattering profiles recorded by image-intensified CCD detectors has been incorporated (Ito *et al.*, 2005). A separate log file records all processing parameters and statistical evaluation results, which are useful in detecting radiation-induced aggregation and/or instrumental instabilities. Nearly all functions in *MarParse* can be switched on and off in the input file. All these tasks are done in one step within a few seconds per image by running the program in command-line mode on a Windows personal computer.

4. Protein solution scattering

Solution X-ray scattering is probably one of the most demanding classes of small-angle scattering studies due to its weak signal level. It requires not only a low level of overall background, but also a high level of instrumental stabilities including those of the X-ray beam and

detector electronics so that intensity scaling and background subtraction are accurately and properly performed. The parasitic scattering, primarily from windows and small air gaps, needs to be minimized in the lowest Q range to obtain accurate X-ray scattering profiles from large proteins and complexes in dilute solutions. In the structural genomics era, the ability to measure protein solution scattering at the lowest possible concentration is important, imposing additional demand for instrumental stability. Here we discuss the solution scattering data obtained from two protein systems to demonstrate the ability of the third-generation instrument.

Streptomyces rubiginosus glucose isomerase is a heterotetramer of total molecular weight 173 kDa (Carrell *et al.*, 1989). It represents a group of moderately large proteins being studied by solution scattering. Fig. 2 shows intensity-scaled X-ray scattering curves recorded at two different protein concentrations. There is no sign of under- or over-subtraction of buffer solution scattering in the subtracted curves, demonstrating the minimum accessible Q value to be approximately 0.0055 Å^{-1} for the protein concentration range typically used. Smaller minimum Q values can be obtained for other classes of specimens such as fibers. Fig. 3 shows the solution scattering of hen egg-white lysozyme (14.3 kDa), which is one of the most extensively studied proteins with the largest number of Protein Data Bank (PDB) entries, and often serves as a benchmark or molecular weight standard for a number of solution X-ray scattering studies. Low protein concentration is essential to avoid interparticle interference (structure factor) when a low ionic strength condition is used. Its relatively small size also makes it challenging to measure the scattering curve accurately at low concentrations. Lysozyme is also prone to aggregate under an X-ray beam. We used a capillary flow cell in combination with the liquid dispenser at a flow rate of 1 µl s^{-1} to minimize radiation-induced aggregation. The merged scattering curve, composed of the low-angle data recorded at the lowest concentration and the higher-angle data recorded at higher concentrations, matches very well with the scattering pattern predicted from the crystallographic structure by *Crysol* (Svergun *et al.*, 1995). The excellent agreement demonstrates that the lysozyme solution scattering is measured at satisfactorily high accuracy even at the lowest concentration point at 0.6 mg ml^{-1}.

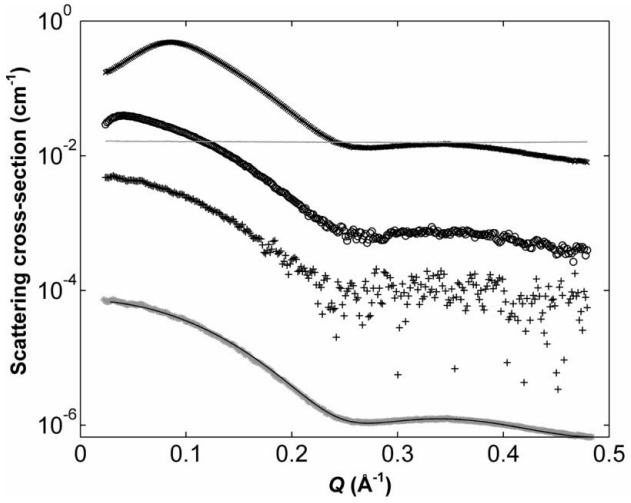

Figure 3
Lysozyme solution scattering recorded at 0.6 (plus signs), 5.2 (circles) and 100 g l^{-1} (crosses) in 1 m*M* acetate buffer at pH 5.0 using the 1 m configuration. A 200 µl aliquot of lysozyme solution was placed in the capillary flow cell in an oscillating motion (1 µl s^{-1}) for the duration of the exposure (20 frames of 30 s). The interparticle interference is clearly seen at 5.2 and 100 g l^{-1} in the low-Q range where the structure factor deviates from unity. The grey flat line represents measured water X-ray scattering, which is used for absolute intensity scaling. Also shown near the bottom of Fig. 3 is the excellent fit of the theoretical scattering curve obtained by *Crysol* using the PDB entry 193L (solid curve) with the merged data (asterisks, displaced along the ordinate to facilitate comparison), which consist of the low-angle data recorded at 0.6 g l^{-1} and the high-angle data recorded at higher concentrations.

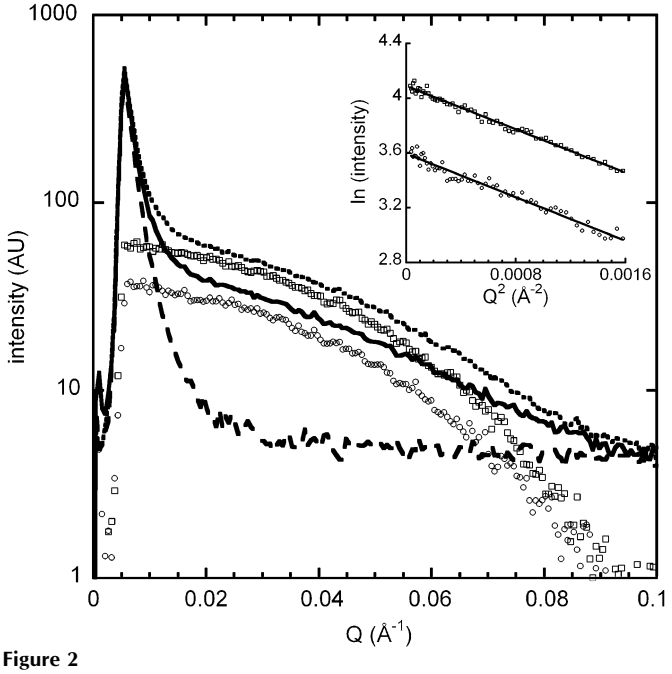

Figure 2
Solution X-ray scattering from *S. rubiginosus* glucose isomerase recorded using the MarCCD165 detector in 10 m*M* HEPES, pH 7.0, 150 m*M* NaCl and 5 m*M* 2-mercaptoethanol at 293 K. The 2.5 m distance and 4 mm beam stop were used. The solid curve was recorded at 1.7 g l^{-1} and the dotted curve at 3.6 g l^{-1}. The dashed curve is the background scattering recorded for a matching buffer solution. Circles and squares represent the net protein scattering for 1.7 and 3.6 g l^{-1}, respectively, after background subtraction. The inset shows the corresponding Guinier plots. The minimum Q value in the Guinier plots is 0.00552 Å^{-1}. The radius of gyration values are 34.0 ± 0.2 Å (1.7 g l^{-1}) and 34.1 ± 0.2 Å (3.6 g l^{-1}).

5. Concluding remarks

The third-generation small-angle scattering instrument on BL4-2 is optimized for structural biology studies. The pinhole camera and the incorporated USAXS setup allow the coverage of scattering angles corresponding to the characteristic lengths from a few ångstroms to one micron. Three types of specialized detectors are available to cover a diverse spectrum of structural studies on macromolecules ranging from randomly oriented to single crystalline samples (Tsuruta, Reddy *et al.*, 1998). A number of specialized sample-handling devices are available for specific sets of scattering/diffraction experiments, including time-resolved studies. The low-Q resolution achieved by the pinhole setup is adequate for a maximum particle dimension in excess of 500 Å and periodic structures whose Bragg spacing is in the range of 1000 Å. The high overall instrumental stability has been achieved to accurately measure protein solution scattering at very low concentrations. The planned optics upgrade and the full field wiggler operation, together with the 500 mA storage ring operation, will make this facility even more effective in a number of structural biology studies. The most up-to-date information on our developments can be found on our web page (Stanford Synchrotron Radiation Laboratory, 2006*b*).

SSRL is operated by Stanford University on behalf of the US Department of Energy, Office of Basic Energy Sciences. The SSRL Structural Molecular Biology Program is supported by the Department of Energy, Office of Biological and Environmental Research, and by the National Institutes of Health, National Center for Research Resources, Biomedical Technology Program. We acknowledge collaboration with SMB staff, in particular, S. McPhillips (*Blu-ICE*), M. George (ICS), A. Aranda (*ImageJ* plug-in), and expert technical support by C. Weidner, K. Sartain, V. Vinetskiy and the SSRL X-ray group. We thank R. Carr for the magnetic sample orienter design.

References

Amemiya, Y., Ito, K., Yagi, N., Asano, Y., Wakabayashi, K., Ueki, T. & Endo, T. (1995). *Rev. Sci. Instrum.* **66**, 2290–2294.

Amenitsch, H., Bernstorff, S. & Laggner, P. (1995). *Rev. Sci. Instrum.* **66**, 1624–1626.

Boesecke, P. & Diat, O. (1997). *J. Appl. Cryst.* **30**, 867–871.

Carrell, H. L., Glusker, J. P., Burger, V., Manfre, F., Tritsch, D. & Biellmann, J. F. (1989). *Proc. Natl Acad. Sci. USA*, **86**, 4440–4444.

Diat, O., Bosecke, P., Ferrero, C., Freund, A. K., Lambard, J. & Heintzmann, R. (1995). *Nucl. Instrum. Methods Phys. Res. A*, **356**, 566–572.

Dubuisson, J. M., Decamps, T. & Vachette, P. (1997). *J. Appl. Cryst.* **30**, 49–54.

Fischetti, R. F., Rodi, D. J., Mirza, A., Irving, T. C., Kondrashkina, E. & Makowski, L. (2003). *J. Synchrotron Rad.* **10**, 398–404.

Fischetti, R., Stepanov, S., Rosenbaum, G., Barrea, R., Black, E., Gore, D., Heurich, R., Kondrashkina, E., Kropf, A. J., Wang, S., Zhang, K., Irving, T. C. & Bunker, G. B. (2004). *J. Synchrotron Rad.* **11**, 399–405.

Gabriel, A. (1977). *Rev. Sci. Instrum.* **48**, 1303–1305.

George, M. J. (2000). *J. Synchrotron Rad.* **7**, 283–286.

Hirai, M., Iwase, H., Hayakawa, T., Miura, K. & Inoue, K. (2002). *J. Synchrotron Rad.* **9**, 202–205.

Ilavsky, J., Allen, A., Long, G. & Jemian, P. (2002). *Rev. Sci. Instrum.* **73**, 1660–1662.

Ito, K., Kamikubo, H., Yagi, N. & Amemiya, Y. (2005). *Jpn. J. Appl. Phys.* **44**, 8684–8691.

Koch, M. H. J., Vachette, P. & Svergun, D. I. (2003). *Q. Rev. Biophys.* **36**, 147–227.

Latimer, M. J., Ito, K., McPhillips, S. E. & Hedman, B. (2005). *J. Synchrotron Rad.* **12**, 23–27.

Levine, L. E. & Long, G. G. (2004). *J. Synchrotron Rad.* **37**, 757–765.

McPhillips, T. M., McPhillips, S. E., Chiu, H.-J., Cohen, A. E., Deacon, A. M., Ellis, P. J., Garman, E., Gonzalez, A., Sauter, N. K., Phizackerley, R. P., Soltis, S. M. & Kuhn, P. (2002). *J. Synchrotron Rad.* **9**, 401–406.

Narayanan, T., Diat, O. & Bosecke, P. (2001). *Nucl. Instrum. Methods Phys. Res. A*, **467**, 1005–1009.

National Institutes of Health (2004). *ImageJ – Image Processing and Analysis in Java*. http://rsb.info.nih.gov/ij/.

Petoukhov, M. V., Eady, N. A., Brown, K. A. & Svergun, D. I. (2002). *Biophys. J.* **83**, 3113–3125.

Rapp, G., Gabriel, A., Dosiere, M. & Koch, M. H. J. (1995). *Nucl. Instrum. Methods Phys. Res. A*, **357**, 178–182.

Stanford Synchrotron Radiation Laboratory (2006*a*). *More Equipments for B-SAXS/D Experiments on BL 4-2*. http://ssrl.slac.stanford.edu/~saxs/instrumentation/more/more.htm.

Stanford Synchrotron Radiation Laboratory (2006*b*). *BL4-2 Biological Small Angle Scattering/Diffraction*. http://ssrl.slac.stanford.edu/~saxs/.

Svergun, D., Barberato, C. & Koch, M. H. J. (1995). *J. Appl. Cryst.* **28**, 768–773.

Tsuruta, H., Brennan, S., Rek, Z. U., Irving, T. C., Tompkins, W. H. & Hodgson, K. O. (1998). *J. Appl. Cryst.* **31**, 672–682.

Tsuruta, H., Reddy, V. S., Wikoff, W. R. & Johnson, J. E. (1998). *J. Mol. Biol.* **284**, 1439–1452.

Wakatsuki, S., Hodgson, K. O., Eliezer, D., Rice, M., Hubbard, S., Gillis, N., Doniach, S. & Spann, U. (1992). *Rev. Sci. Instrum.* **63**, 1736–1740.

Zuo, X., Cui, G., Merz, K. M. Jr, Zhang, L., Lewis, F. D. & Tiede, D. M. (2006). *Proc. Natl Acad. Sci. USA*, **103**, 3534–3539.